Role of atomic hydrogen supply on the onset of CO_2 methanation over La-Ni based hydrogen storage alloys studied by *in-situ* approach

Keito Sawahara[1*], Kohei Yatagai[1+], Torben Boll[2,3], Astrid Pundt[3], Ryota Gemma[1,4*]

[1] Graduate School of Engineering, Tokai University, Kanagawa, Japan

[2] Karlsruhe Nano Micro Facility (KNMF), Karlsruhe Institute of Technology, Eggenstein-Leopoldshafen, Germany

[3] Institute for Applied Materials – Materials Science and Engineering (IAM-WK), Karlsruhe Institute of Technology, Karlsruhe, Germany

[4] Micro/Nano Technology Center, Tokai University, Kanagawa, Japan

[*]Corresponding authors

[+] Current address: Production Department, Equipment Division, Ebara corporation, Tokyo, Japan

Abstract

Mechanochemical CO_2 methanation reactions using $LaNi_5$ and $LaNi_{4.6}Al_{0.4}$ hydrogen storage alloy powders were investigated by the *in-situ* monitoring of the gas pressure change during ball-milling. Methane generation begins when the H_2 partial pressure drops due to the H-uptake by the powder. Phase transition occurred in the sample after milling for 15 min and 224 min, with separate metallic Ni, La-oxide and La-hydroxide phases observed. Methane generation continued even after this phase separation. Our results imply that the formation of La-hydroxide at the surface and sub-surface contributed to methane generation during ball-milling. A comparison of $LaNi_5$ and $LaNi_{4.6}Al_{0.4}$ quantities suggests the amount of hydrogen stored in the hydrogen storage powder dominates the timing of the onset of the methane generation.

Introduction

Since global warming is proceeding more rapidly than anticipated, the need for radical reductions in CO_2 emissions has become more pressing. One approach which has been suggested is to capture and utilize CO_2 [1–4] by forming CH_4 [5–7] using a process known as the Sabatier reaction (CO_2 methanation reaction). In this process, CH_4 can be generated from hydrogen produced from water electrolysis. This can be done using renewable energy and either atmospheric CO_2 or exhausted CO_2 directly from carbon-based fuel combustion sites.

According to the suggested reaction for the Sabatier reaction, high temperatures in the range of 300 ^oC ~ 400 ^oC are required in the presence of a catalysts like Ni [8,9].

$$CO_2 + 4H_2 \Leftrightarrow CH_4 + 2H_2O \qquad \Delta H^o_{298\ K} = -165\ kJ/mol \qquad (1)$$

Significant research effort has been dedicated to the search for more active catalysts, with the main focus on Ni-based catalysts supported on different metal oxides [10–18] e.g. Ni/Al_2O_3[19–24], sponge Ni/CeO [25] and Ni/ZrO_2 [26–31]. Methanation of CO_2 using $LaNi_5$ powder was first reported by Ando et al. in 1999 [32]. Recently, Rivero-Mendoza *et al*. reported the catalytic activity of the La-Ni/γ-Al_2O_3 catalyst/support upon the CO_2 methanation reaction [33], with the generation of catalytically active Ni/LaOx interfaces during the reaction. The drawback of this study was that a reaction temperature of over 350 ^oC was required to reach a CO_2 conversion rate of higher than 80%.

In a recent report by Hirata and Fukuhara [34,35] it was revealed that a small amount of O_2 in the inlet gas mixture automatically initiates the methanation reaction at much lower temperatures of about 50 ^oC. The heat of formation of water increases the catalyst surface temperature to about 500 ^oC, which was sufficient to drive the methanation reaction. It is also possible to reduce the reaction temperature by a mechanochemical reaction. In 1996, Mori *et al*. reported a mechanochemical CO_2 methanation reaction by the ball-milling of Ni, Fe or Ru together with MgO in a $CO_2 + H_2$ atmosphere [36].

In earlier studies by our group, we have reported on the CO_2 methanation reaction by the ball-milling process using $LaNi_5$ alloys [37–39]. The ball-milling of $LaNi_5$ powder in a mixture of $CO_2 + H_2$ gases was found to successfully result in CH_4 generation. Upon the CO_2 methanation reaction, the $LaNi_5$ was found to form a decomposed nanostructure of nanocrystalline Ni-particles embedded in different lanthanum compounds, including La-oxides, La-hydroxides and La-hydroxycarbonates [37]. This kind of decomposition was confirmed by atom probe tomography (APT) to be phase separation, where the resultant nanostructure showed phase separation at a scale of several tens of nanometers after the mechanochemical methanation reaction [37]. A comparison of the thermally driven methanation processes with the methanation reaction driven by mechanochemical methanation is expected to reveal the impact of the decomposed nanostructure on the methanation reaction (mechanochemical methanation).

In 1977, Soga *et al.*[40] investigated the impact of atomic H supply from $LaNiH_x$ hydride on the hydrogenation of ethylene to form ethane and showed that the kinetics of the hydride were faster than those of the $LaNi_5$. Similarly, the hydrogenation of acethylene and propyne over hydrogenated ErNix was observed by Tsukuda *et al*. [41]. Kato *et al*. [42] discussed the effect of an atomic H-supply to a ZrCo hydrogen storage alloy on the CO_2 methanation reaction. They conducted a ToF-SIMS analyses and concluded that the reduction of surface Co-oxide is crucial to provide a fresh metal surface and an atomic H supply for the methanation reaction [40]. In both the reduction of CO_2 and the oxide, it has been reported that the atomic H-supply from the hydride phase was either directly or indirectly required for methanation [42]. The ball-milling process naturally offers newly created fresh surfaces of the milled powder by its own, which offers active reaction sites for the gas-solid reaction.

In this study, we investigate the generality of the effect of atomic H supply from a bulk material by using ball-milled La-Ni based alloys like $LaNi_5$ and $LaNi_{4.6}Al_{0.4}$. In an earlier study, a phase separation into metallic Ni and La-compounds was observed by atom probe analysis in the course of the mechanochemical process [37]. Upon the phase separation, it is assumed that H is desorbed when a bulk H-solid solution phase is present. Even though the initial surface of these alloys is oxidized, we assume that the desorption of H creates available sites for the reaction. The hydrogen solubility of $LaNi_{4.6}Al_{0.4}$ is superior to that of $LaNi_5$ (at the same H_2 pressure). Because more

hydrogen is in the solute phase, more atomic H-supply for methanation is potentially available in the $LaNi_{4.6}Al_{0.4}$ alloy than $LaNi_5$. That is, assuming the atomic H supply directly plays a role in the methanation reaction, these two alloys differ substantially.

Herein, we investigated the impact of the atomic H supply on the mechanochemical CO_2 methanation reaction on $LaNi_5$ and $LaNi_{4.6}Al_{0.4}$ by the *in-situ* monitoring of the reacting gases. We discuss the related sequences of phase separation responsible for methane generation.

Experimental

Sample preparation and mechanochemical CO_2 methanation experiment

Lumps of $LaNi_5$ (Sigma Aldrich) were crushed and sieved down to particle sizes of 53 – 75 µm. The $LaNi_{4.6}Al_{0.4}$ powder (The Japan Steel Works, LTD) was pulverized in a hydrogen atmosphere to particle sizes of below 45 µm. A homemade high-pressure Sieverts' type apparatus and a vibratory ball-milling apparatus (Nissin Giken NEV-MA-8) were connected in order to introduce H_2 gas and CO_2 gas separately and to monitor the pressure inside the vial. Right at the top of the vial, a gas sampling port with plastic septum was mounted to sample the gas with a micro-syringe to allow for gas composition analysis. The gas inside the vial was analyzed by gas chromatography (GC, Shimadzu GC-14B) with a thermal conductivity detector (TCD). The

carrier gas was 99.99% N_2 with a flow rate of 40 ml / min. A packed column of Shincarbon ST from Shinwa Chemical Industries Ltd, was used. The temperature at the injector, the detector and the column was set to 150 ºC, respectively. The gas composition was calculated by taking into account the gas sensitivity factor determined by calibration measurements using standard gases.

Fig. 1 shows a schematic picture of the experimental set up. $LaNi_5$ or $LaNi_{4.6}Al_{0.4}$ powder (0.500 g each) together with ten balls (10 mm-diameter) made of SUS304 were placed in a vial made of SUS304. The vial interior was then evacuated below 5 Pa by an oil rotary pump (Hitachi Co. Ltd.), followed by the injection of H_2 (Purity: 7N) and CO_2 (Purity: 99.5%) gas using the Sieverts' type apparatus. The ratio of CO_2 and H_2 was 1 : 1, which is off the ratio of Sabatier reaction (see Eq.1) to allow for detection of least-sensitive CO_2 by the TCD. Before ball-milling, the initial gas composition was checked by GC.

During ball-milling, the gas pressure was measured by Sieverts' type apparatus and the gas composition was analyzed by GC intermittently. A vibratory ball-milling apparatus was used at a vibration frequency of 11.7 Hz for 0.25 h – 224 h. The vial temperature was kept at 20 ℃ by running water during milling. Detailed milling conditions are summarized in Table. 1.

Table. 1 Ball-milling conditions

Sample powder	$LaNi_5$ or $LaNi_{4.6}Al_{0.4}$
Mill type	Vibratory mill (Nissin Giken NEV-MA-8)
Material of vial/balls	SUS304
Vial capacity	148 cc
Diameter and number of balls	10 mm, 15 pieces
Total weight of the sample	0.500 g
Vibration frequency	11.7 Hz
Milling period	0.25 h – 224 h
Atmosphere	H_2 + CO_2, or pure H_2, or pure CO_2

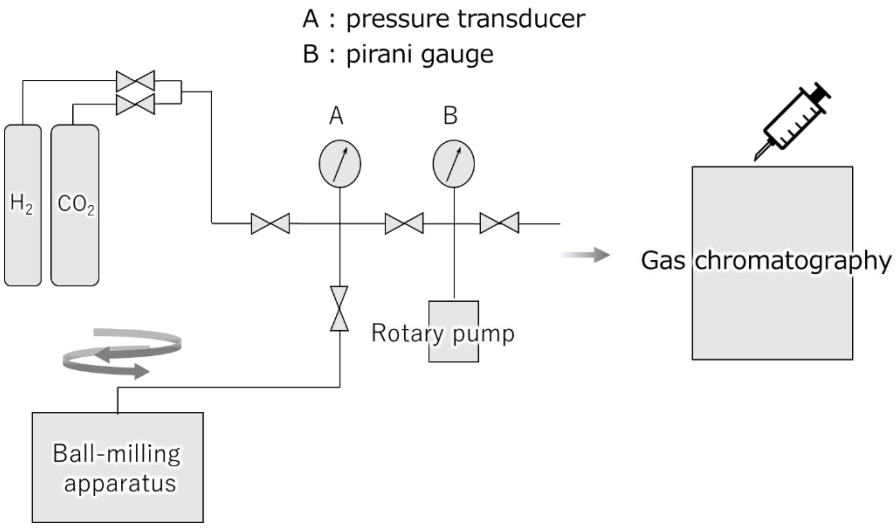

Figure 1 Schematic drawing of the experimental apparatus. A homemade Sieverts' type apparatus is connected with a vibratory ball-milling apparatus. The sample is hosted in the ball-milling apparatus.

Characterization of powder sample

Phase identification of the milled powder was carried out by X-ray Diffraction (XRD) using Rigaku, Miniflex 600 (40 kV, 15 mA, Cu K_α with λ= 0.15405 nm). The particle sizes and elemental compositions of the powder samples before and after milling were examined by Scanning Electron Microscope (SEM) and Energy Dispersive X-ray Spectroscopy (EDX) with JEOL, JSM-7100F. The surface of the powder samples was analyzed by X-ray photoelectron spectroscopy (XPS) with ULVAC-PHI, PHI Quantera II (Al Kα with 1486.6 eV). The spectra fitting and peak separation treatment were performed using PHI Multipak (ULVAC-PHI). The O1s and La3d spectra were fitted with gaussian / Lorentzian line shapes and a Shirley background.

Results and discussion

Gas composition analysis

Fig. 2 shows the results of the gas composition analysis by GC during ball-milling of $LaNi_5$ in H_2 and CO_2, after different milling times. A peak of CH_4 starts to appear after milling for 3 h (Fig. 2 (b)). After milling for 24 h, the CO_2 peak totally disappears, and only H_2 and CH_4 peaks remain (Fig. 2 (c)). Further ball-milling resulted in even more pronounced CH_4 generation (Fig. 2 (d)). These results hint that CO_2 was consumed by the forming of carbonates, for example.

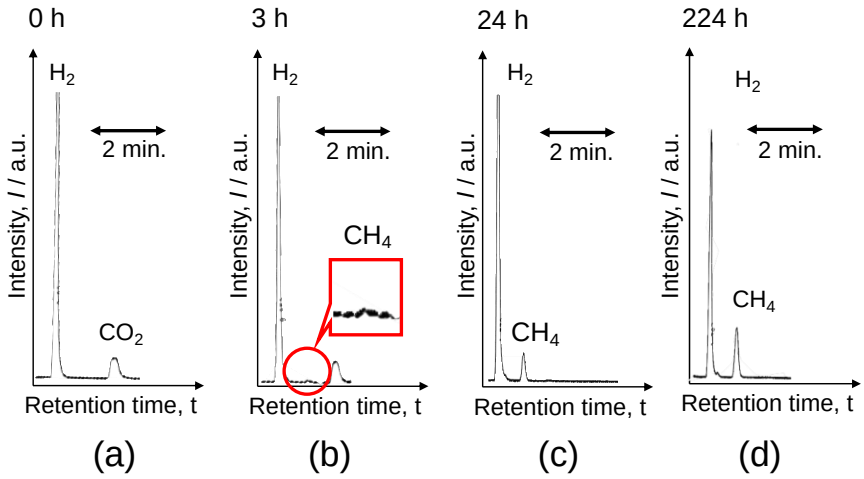

Fig. 2 GC results obtained during ball-milling of $LaNi_5$ (0.500 g) under CO_2 and H_2 atmosphere with ball-milling times of (a) 0 h, (b) 3 h, (c) 24 h, (d) 224 h.

Gas pressure analysis

The result of *in-situ* pressure monitoring analysis during ball-milling of $LaNi_5$ is shown in Fig. 3. A characteristic change in pressure at early periods of ball-milling (1 h ~ 4 h) was observed, as shown in Fig. 3 and its inset. At the period of 0 – 1 h, the total pressure abruptly decreased, followed by temporarily increase within the period of 2 – 4 h. Further milling again causes gradual

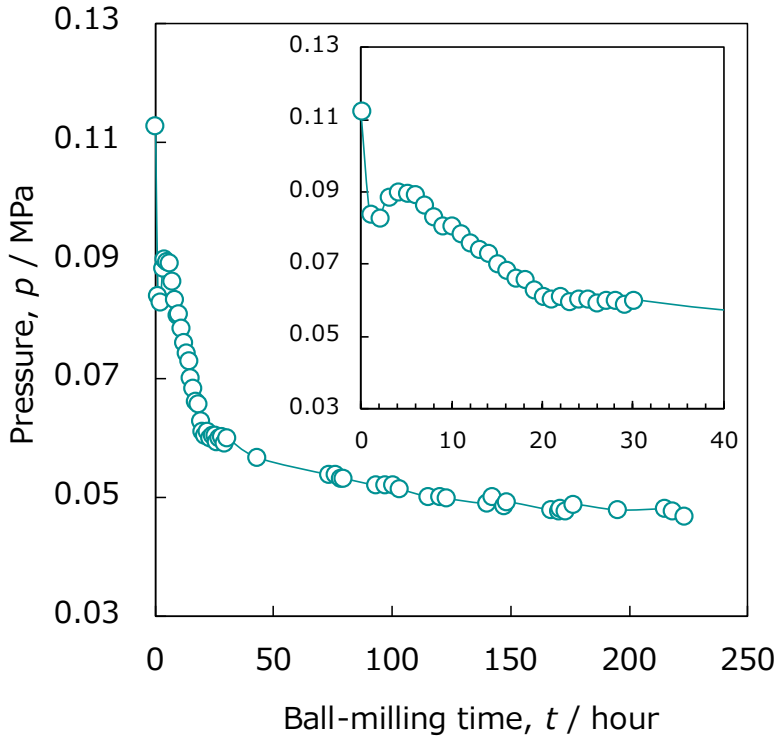

pressure drop with time, while the pressure tends to stabilize when the milling time exceeds 20 h. This suggests that the mechanochemical CO_2 methanation reaction has actively progressed until the milling time of 20 hours.

Fig. 3 Change of gas pressure obtained during ball-milling of 0.500 g $LaNi_5$ powder under CO_2 and H_2 atmosphere. The inset shows the reaction behavior of early stage until 40 hours.

Change of gas composition

Fig. 4 shows the change of gas composition during the ball-milling process. The gas composition was carefully examined by using results of gas composition analysis by GC and gas pressure analysis as obtained in Fig. 3. It is clearly shown in Fig. 4 that the initial pressure drop observed in Fig. 3 was due to decrease of the H_2 gas present in the milling vial. This might be due to the milling-induced hydrogen absorption by $LaNi_5$, since newly created surfaces by milling are typically active for H-uptake. Another possibility could be H_2O formation, as the Sabatier reaction involves the formation of H_2O. It was determined, however, that this was not the case since no CH_4 formation had been observed at this point: this should occur simultaneously with the H_2O formation. Moreover, the observed pressure drop of H_2 takes place even if the ball-milling is conducted in pure H_2 atmosphere (Supplementary, Fig. S1). This suggests that the H_2 pressure drop is mainly due to the hydrogen uptake of the $LaNi_5$ alloy powder.

It was found that the H_2 pressure gradually increases after this observed pressure drop of H_2. This sluggish behavior could be H_2 desorption from $LaNi_5$ due to the mechanical impact and the concomitant temperature increase of the powder. Another possibility is the decomposition of H_2O. Once formed H_2O, by the Sabatier reaction can decompose into hydrogen and oxygen by ball-milling process using balls and vial made of stainless steel, as reported by Sawama *et al*.[43]. The reported water decomposition was considered as a result of oxidation reaction of Fe and Cr in the

SUS304 powder which was scrubbed by the milling process, thereby a small amount of H_2 is emitted as gas [43]. That is, the gradual observed increase in H_2 pressure in our study could be the result of such water decomposition. This should, however, induce oxidation of the $LaNi_5$ powder at the same time. Eventually, a complex nanostructure with metallic Ni embedded in La-compounds emerges, as observed by APT [37]. Note that as this powder sample is in the process of being phase decomposed, CH_4 generation remains active, as the amount of CH_4 continues to increase with prolonged ball-milling time. The same trend was observed when $LaNi_{4.6}Al_{0.4}$ was similarly ball-milled (Supplementary S2). This is probably because the metal/oxide nano-composites are analogue to the conventional catalyst as a result of the mechanochemical process itself, which may have allowed catalytic CO_2 methanation without further compositional change of the original alloy phase to have continued.

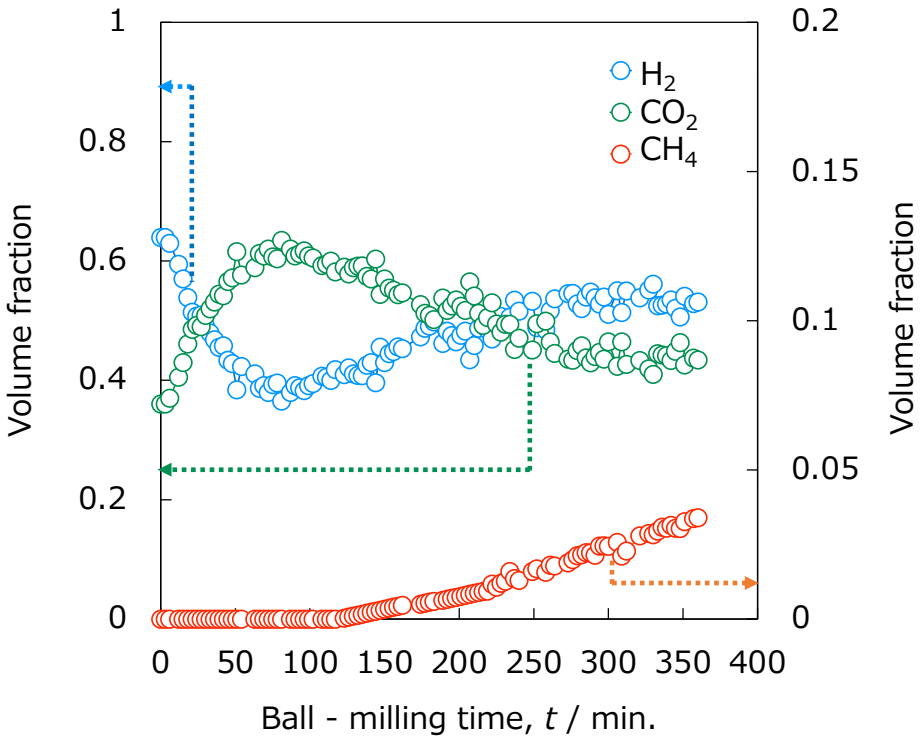

Fig. 4 Change of gas volume fraction during mechanochemical CO_2 methanation reaction over $LaNi_5$ under a CO_2 and a H_2 atmosphere. The H_2 content in the gas mixture shows a drastic decrease before 70 min., and then gradually increases. The sum of CO_2 and H_2 should be 1.

XRD

The crystal structure of the milled $LaNi_5$ powder was characterized by XRD. Fig. 5 shows the XRD results of the powder milled in the H_2 + CO_2 atmosphere after different milling periods. Also included are some reference pattern positions, marked with red triangles ($LaNi_5$, green dots (La-oxide/hydroxide or carbonate) and Ni (stars) [44–49]. Milling for 15 min results in peak broadening, but still verifies the original structure of $LaNi_5$. After milling for 45 min, the powder shows a trace of phase separation, indicating a weak Ni peak at around 44°. Further milling results in even more pronounced phase separation, as Ni peaks clearly start to grow with increasing ball-milling time. The small hump visible at around 29° could be assigned to the strongest peak of La_2O_3 or other La-compounds. It is likely that La is in the form of a fine oxide, hydroxide or carbonate state, maybe at the nanometer scale, and therefore cannot be unambiguously separated by XRD measurements. A similar phase separation of the $LaNi_5$ powder was also confirmed by Yatagai *et al*. [37] in their experiment using planetary ball-mill.

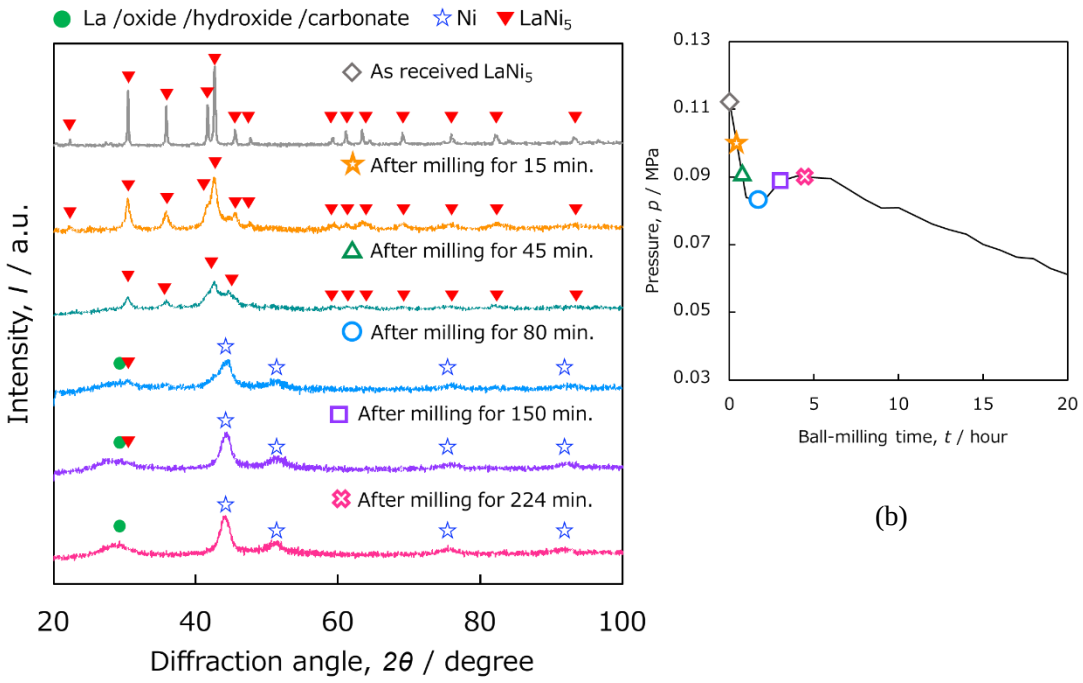

(a) (b)

Fig. 5 (a) XRD patterns of $LaNi_5$ after milling for 224 min., 150 min., 80 min., 45 min. and 15 min. Reference peak positions of Ni (blue open star) [46], La [47], $La_2O_2CO_3$ [49], La_2O_3 [44], $La(OH)_3$ (green filled circle) [48] and $LaNi_5$ (red filled triangle) [45] are indicated together. (b) Corresponding sequence of pressure change during ball-milling, indicating each time (15 min. – 224 min.) where XRD measurements were carried out as marked by different symbols. A Ni-phase becomes visible after milling for 45 min.

SEM-EDX

The SEM images of unmilled (Fig. 6 (a)) and ball-milled $LaNi_5$ powder samples after milling for (b) 15 min, (c) 80 min, (d) 150 min and (e) 224 min, respectively, are shown in Fig. 6. According to Fig. 6, the particle size of the as-received sample $LaNi_5$ powder was 53-75 μm. These large particles were pulverized down to several tens of μm in a short milling period of 15 min. Prolonged milling reduces the large particle size only to some extent. Indeed, ball-milling for 224 min did not result in significant particle large size reduction. Rather, the agglomeration of the particles becomes visible. In between the large particles, a powder with particles sizes of less than 5 μm, can be seen. These tiny particles also cover the larger particles. The particle size distribution looks broad (Supplementary S3), suggesting a bimodal distribution.

Note that an abrupt H_2 pressure drop was observed in the period of 0 ~ 80 min (Fig. 4). In this same period, the large particle size reduction was also significant, and few small particles remain.

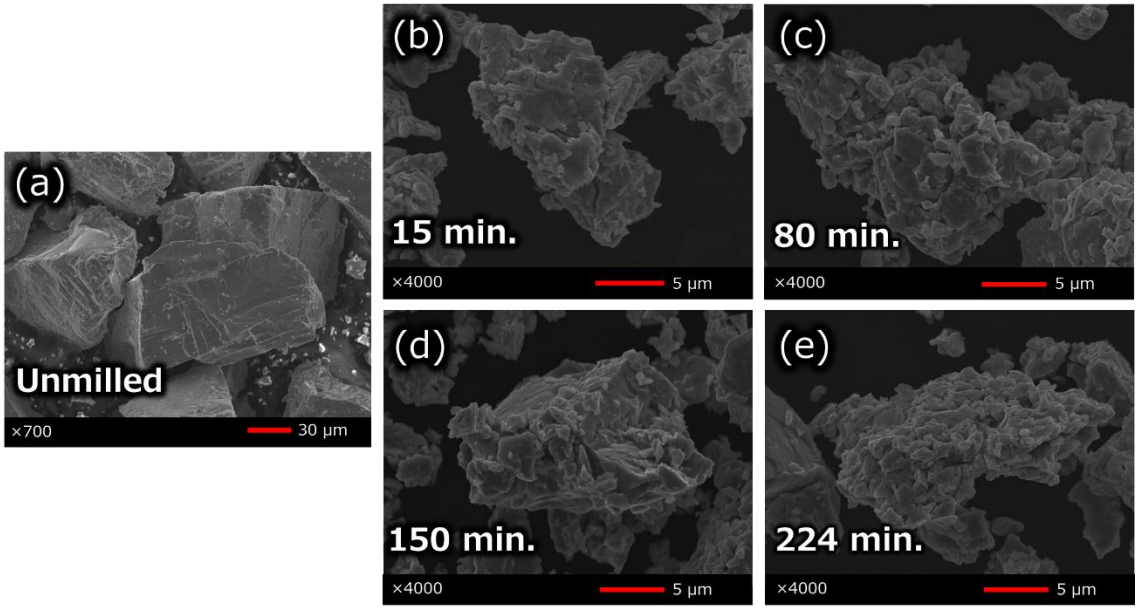

Fig. 6 SEM image of as received sample (a) and powder samples after milling for (b) 15 min, (c) 80 min, (d) 150 min and (e) 224 min. After ball-milling, particle sizes obviously decreased, but extended ball-milling over 70 min did not result in efficient particle size reduction of the larger particles.

It is well known that ball-milling often induces sample contamination [50]. In our study, contamination from the SUS304 balls and vial was confirmed, as shown in Figure 7. Except for the partial segregation of Fe within the shown particle, Fe was distributed homogeneously throughout the entire particle.

While the prolonged milling time did not result in the drastic particle size reduction of the larger particles, greater Fe contamination was found, as indicated in Table. 2 and Fig. 8. The Fe and Cr concentration exceeded 50 at.% and 16 at.%, respectively, after 24 hours of ball-milling. The increase of Fe and Cr concentration is monotonic with time. Between 24 h and 224 h, no significant difference was found between c_{Fe} and c_{Cr}, nor was the difference in the sizes of the large particles significant (Fig. 6). This could be due to the effect of mechanical impact absorption by contaminant particles from the SUS304 balls and vial. It is assumed that the sample powder and SUS contamination from the vial and balls behave like a buffer agent [51] as the ball-milling time increases. Hence, the sample powder was less likely to be pulverized and contaminated after long ball-milling for 24-224 hours.

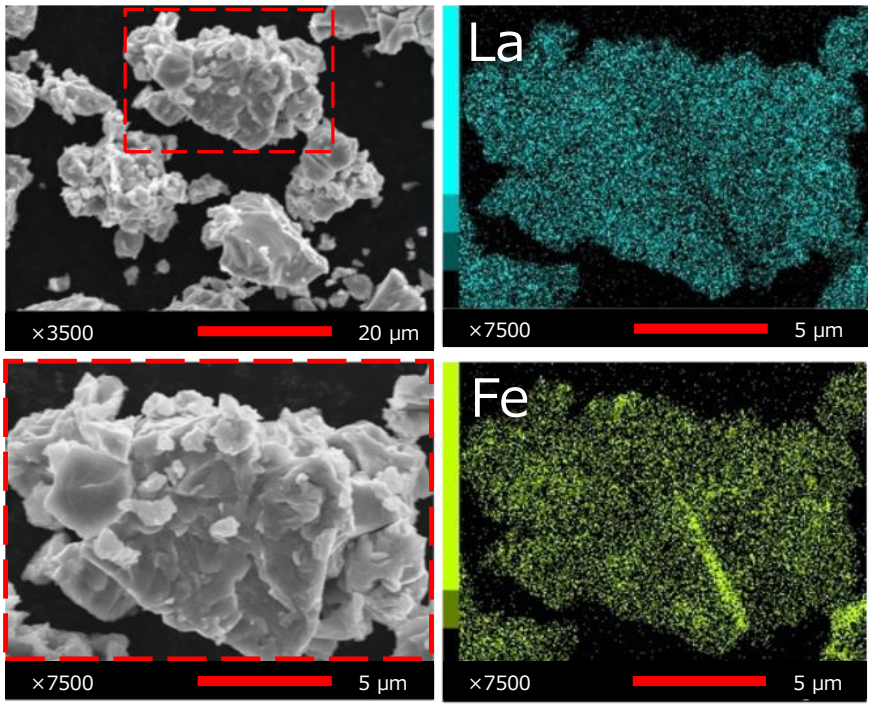

Fig. 7 EDX mapping images of $LaNi_5$ powder sample after milling for 150 min.

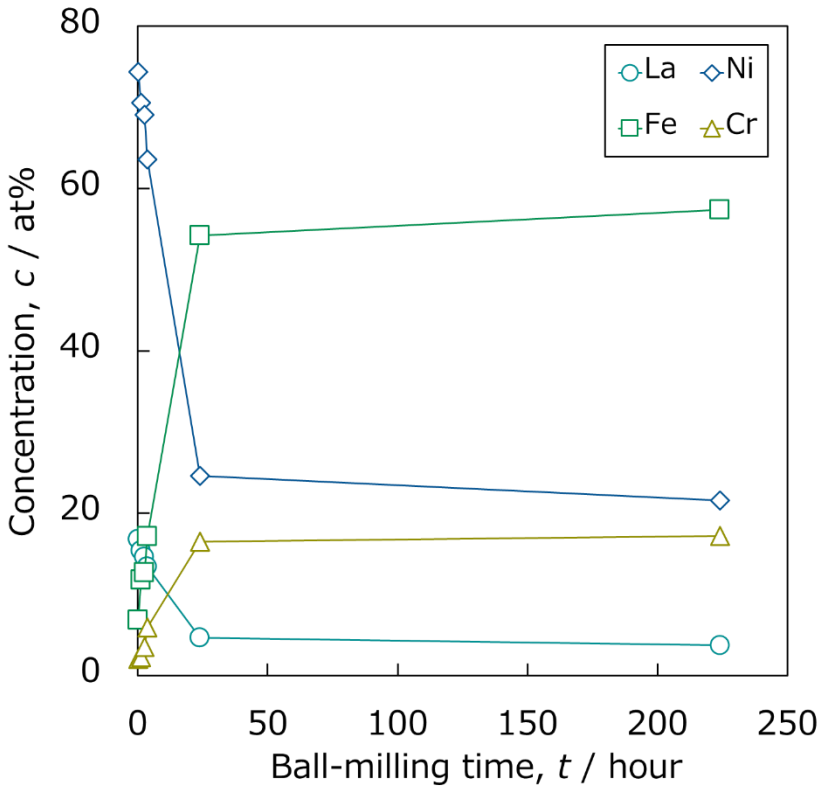

Fig. 8 Change of sample composition. The composition stabilizes after milling for 24 hours.

Table. 2 Results of semi-quantitative analysis of sample composition at each period of ball-milling under $CO_2 + H_2$

Ball-milling time	La	Ni	Fe	Cr
15 min.	16.8	74.4	6.8	2.0
80 min.	15.4	70.6	11.8	2.2
150 min.	14.6	69.1	12.7	3.6
224 min.	13.4	63.6	17.1	5.9
24 h	4.7	24.6	54.2	16.5
224 h	3.8	21.6	57.4	17.2

XPS

In air, the surface of $LaNi_5$ tends to form lanthanum oxide and hydroxide [52]. Moreover, in the presence of water and CO_2, lanthanum oxide forms hydroxide and carbonate, respectively [52]. Because the XPS La $3d_{5/2}$ spectra have well separated spin-orbit components [53], the Lanthanum chemical bond can be assigned by the different splitting of these twin peaks. It has been reported that the width of the La $3d_{5/2}$ twin peaks have a splitting width of about 3.5 eV [54,55], 3.9 eV [52,56,57] and 4.6 eV [52,53,55–62] for lanthanum carbonate, hydroxide and oxide, respectively.

Figure 9 shows the La $3d_{5/2}$ spectra obtained from the as prepared sample and the sample after milling for different periods. Reference values of the binding energy and the width of the twin peaks (ΔB.E.) of $La3d_{5/2}$ reported in the literature are listed in the supplementary information (Table S1) with the experimental values from this study. In this study, the ΔB.E. of the as-prepared sample at the surface was 3.58 eV. This implies that the initial surface of $LaNi_5$ consists of La-carbonate (e.g. $La_2(CO_3)_3$: ΔG° = -3141 kJ/mol [63]) together with La_2O_3. This may be because the sample was stored under an atmospheric dry air condition. However, the XRD measurements did not show any clear indication of carbonates: this was probably due to the extremely thin carbonate layer on the surface.

After milling for 15 min (where the abrupt pressure drop shown in Fig. 2 was recorded), the chemical state of the surface has changed to a hydroxide-like state (ΔB.E. = 3.78 eV). After further

milling for 150 min, the same hydroxide-like state at the surface (ΔB.E. becomes larger) still holds, and the peak height decreased. We should note that methane generation occurs at this point (see Fig. 4). CO_2 methanation and concomitant water formation at the surface is suggested here. Even longer milling for 224 min, however, indicated again higher peaks, while the ΔB.E. was almost the same value as that of 150 min.

The chemical state below the top surface (sub-surface) was somewhat different. Fig. 9 (b) shows the spectra obtained after sputtering for 3 min with 2 kV Ar ion. The as-received sample shows ΔB.E. of about 4.03 eV, which suggests the presence of hydroxide. The chemical state seems to hold similar sate (ΔB.E. = 3.79 eV) even after milling for 15 min, showing the same trend as the top surface state (Fig. 9). However, the chemical state below the surface changes to an oxide-like state after milling for 150 min, where the ΔB.E. broadens to 4.34 eV. This was not seen at the top surface: the top surface was hydroxide-like at this stage according to the spectrum in Fig. 9 (a). Interestingly, this stage corresponds to where the onset of methane generation was observed (Fig. 4). Extended milling time (extended reaction time) ends up with the chemical state below the surface showing ΔB.E. = 4.1 eV, which could be interpreted as both oxide and hydroxide. The spectra of O1s (Supplementary Fig. S4) also suggests the above-mentioned trend of chemical states both at the surface and in the sub-surface.

La_2O_3 is hygroscopic and forms $La(OH)_3$ under the presence of water. Water should be present during the milling in the current study if Eq.(1) is assumed, which would result in the conversion of La_2O_3 to $La(OH)_3$. It seems unlikely that the hydroxide state (e.g. $La(OH)_3$; ΔG^o = -1278 kJ/mol) [63] and oxide state (e.g. La_2O_3: ΔG^o = -1705 kJ/mol) [63] switches back and forth near the powder surface in the course of milling time, because the dehydration reactions of $La(OH)_3$ to LaOOH and 2LaOOH to La_2O_3 occur at above 330 ^oC and 550 ^oC, respectively [64]. These temperature ranges are much higher than those in our experiment. We speculate that the observed coexistence of La-oxide and La-hydroxide could be a result of non-equilibrium state induced by mechanochemical reaction as often observed in different metal oxide systems where oxides could be reduced by ball-milling (for example) [65]. Water molecules generated from dehydrated La-hydroxide could then also be reduced by the mechanochemical process in a similar manner as that reported in an earlier study [43], yielding H_2, which might be considered as an additional H-supply for CO_2 methanation.

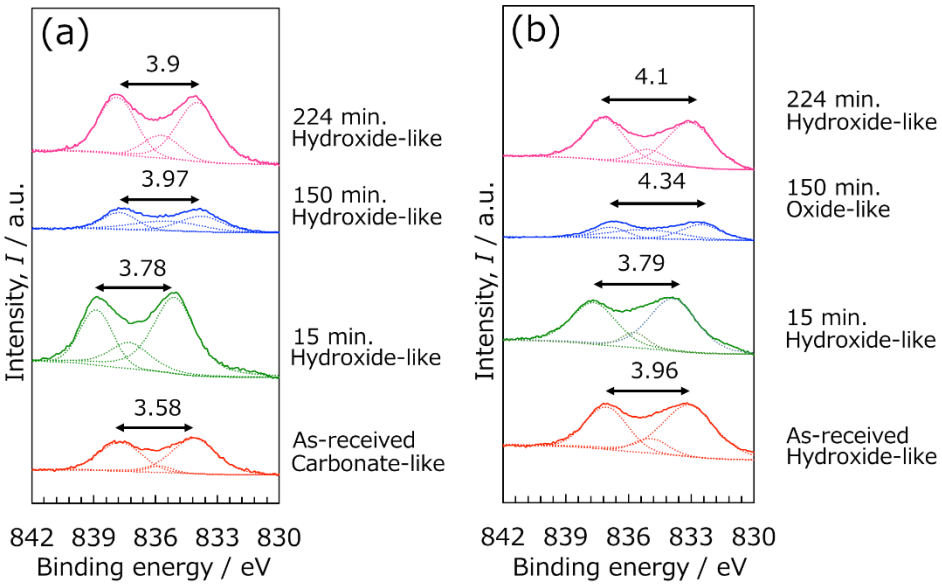

Figure 9 XPS spectra around $La3d_{5/2}$ obtained from $LaNi_5$ powder after mechanical CO_2 methanation experiments at different milling periods (a) top surface (b) sub-surface, after sputtering for 1 min by 2 kV Ar^+.

$LaNi_5$ vs. $LaNi_{4.6}Al_{0.4}$

$LaNi_5$ and $LaNi_{4.6}Al_{0.4}$ have different H-solubilities at similar H_2-partial pressures. In our experiment on $LaNi_5$, the initial partial pressure of H_2 in the vial was 0.05 MPa. At this H_2 pressure and at 293 K, the equilibrium H solubility in $LaNi_{4.7}Al_{0.3}$ is 5.8 times larger than that of hydrogen in $LaNi_5$, as reported by Suzuki *et al*. [66]. That is, that the atomic H supply for $LaNi_{4.6}Al_{0.4}$ is greater than that of $LaNi_5$.

The change of the gas composition (H_2 and CH_4) over the reaction time is shown in Fig. 10 in the normalized scale, as recorded by the *in-situ* pressure monitoring of $LaNi_5$ powder and $LaNi_{4.6}Al_{0.4}$ powder. The trend is similar in both cases; H_2 is mainly consumed within the first several minutes and the H_2 partial pressure continues to decrease for a time span of 50 min, and then increases again before stabilizing at a certain value. Methane generation occurs at around 120 min in case of $LaNi_5$, while the reaction in $LaNi_{4.6}Al_{0.4}$ is faster, with methane generation starting at around 70 min. The observed drop in the H_2 amount in both samples can be compared at the normalized scale shown in Fig. 10. Clearly, early stage H_2 consumption is larger for $LaNi_{4.6}Al_{0.4}$ than for $LaNi_5$, as indicated by the green curve, which lays below the purple curve. This is due to the larger H-solubility of $LaNi_{4.6}Al_{0.4}$ than $LaNi_5$ and should result in a higher amount of atomic hydrogen being available for the subsequent methanation reaction. This once absorbed atomic H can be pushed out from the internal regions by the mechanical impact during

the milling process and concomitant heat dissipation. It may also contribute to the phase separation at later stages. Hence, the suggested mechanism of atomic H supply suggested by Kato *et al*. for the methanation reaction on ZrCo should be valid also in the case of mechanochemical CO_2 methanation on La-Ni alloys at least at its onset. Prolonged ball-milling induces the phase separation of the $LaNi_x$ alloy into Ni and different La-compounds, mainly including La-oxides. It is assumed likely that the Ni/Oxide interfaces which resemble normal catalyst/support composites are also responsible for further mechanochemical CO_2 methanation.

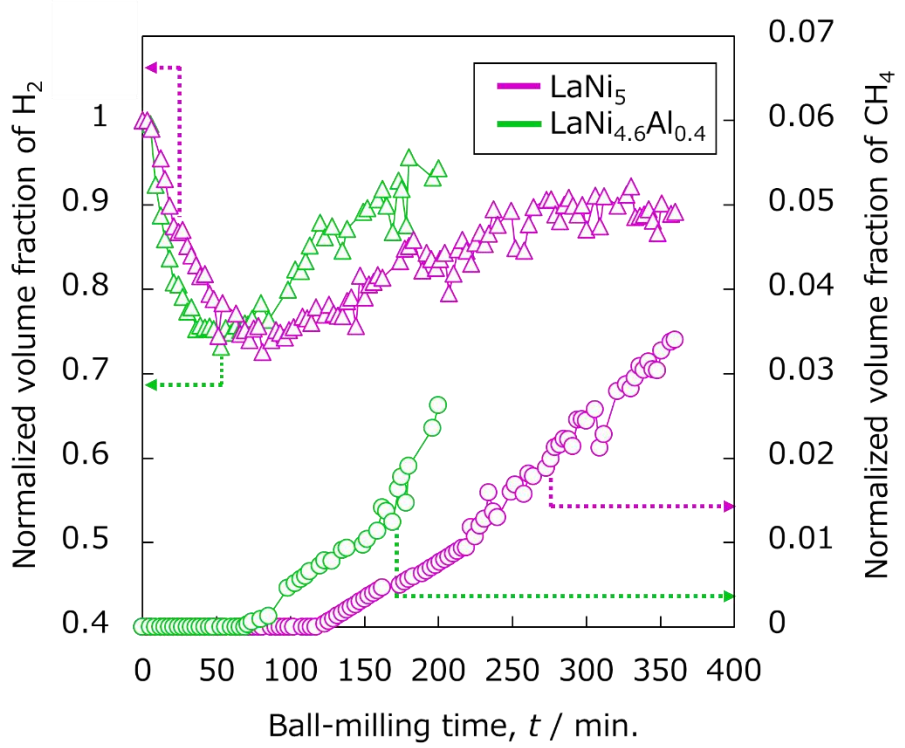

Fig. 10 Change of normalized volume fraction of H_2 and CH_4 during mechanochemical CO_2 methanation by ball-milling of $LaNi_5$ or $LaNi_{4.6}Al_{0.4}$ powder under H_2 + CO_2 mixture gas.

Summary

In this study, we reported the *in- situ* monitoring results of CO_2 methanation reaction over La-Ni based alloy powders by mechanochemical ball-milling in a mixture CO_2 and H_2 gases. CH_4 was generated after milling the alloy powders for 3 hours. CO_2 completely disappeared from the gas mixture after milling for 24 hours, suggesting La-carbonate formation, as indicated by the XPS results. Notably, CH_4 continued to be yielded even after the disappearance of CO_2 in the reaction vial. This suggests that these carbonates are carbon sources for the mechanochemical methanation reaction, as was suggested in our previous study. After milling for 15 min and 224 min, the sample formed La-hydroxide. These results indicate that the formation of La-hydroxide at the surface and sub-surface likely has a positive impact on methane generation by ball-milling, where various non-equilibrium mechanochemical reactions could be involved. This aspect requires more attention as a future research topic.

The *in-situ* pressure measurements revealed a characteristic pressure drop at the early stages of the reaction: this was the result of hydrogen being consumed most probably due to the hydrogen uptake by the alloy powder. This is underpinned by Kato *et al*. by the faster hydrogen pressure drop for $LaNi_{4.6}Al_{0.4}$ than for $LaNi_5$ due to the large difference in H-solubility. Moreover, the initiation of CH_4 generation was earlier for $LaNi_{4.6}Al_{0.4}$ than in the case of $LaNi_5$. Thus, hydrogen atoms once absorbed in the alloy powder are continuously supplied to the alloy surface by

subsequent phase separation during ball-milling, thereby resulting in the faster initiation of the methanation reaction. While CH_4 generation is being initiated, La-oxide was detected in the bulk region by both XRD and XPS results, hinting at the onset of phase separation. This also supports the hypothesis that the H-supply from the La-Ni based hydrogen storage alloys is accountable for CO_2 methanation. Our results suggest that the mechanism is of general nature. At the same time, however, a phase decomposed structure with a Ni/Oxide interface resembling a usual catalyst composite is naturally established. This interface contributes to the CO_2 methanation mechanochemically, since methane generation continues with ball-milling time.

Acknowledgement

This work was partially supported by financial support from Research and Study Project of Tokai University Educational System General Research Organization and Japan Society for the Promotion of Science (JSPS) KAKENHI via Grant Number JP19K15683. Authors would like to thank the Imaging Center for Advanced Research in Tokai University.

References

[1] Aresta M, Dibenedetto A. Utilisation of CO2 as a chemical feedstock: opportunities and challenges. Dalton Transactions 2007:2975–92. https://doi.org/10.1039/B700658F.

[2] Graves C, Ebbesen SD, Mogensen M, Lackner KS. Sustainable hydrocarbon fuels by recycling CO2 and H 2O with renewable or nuclear energy. Renewable and Sustainable Energy Reviews 2011;15:1–23. https://doi.org/10.1016/J.RSER.2010.07.014.

[3] Hoekman SK, Broch A, Robbins C, Purcell R. CO2 recycling by reaction with renewably-generated hydrogen. International Journal of Greenhouse Gas Control 2010;4:44–50. https://doi.org/10.1016/J.IJGGC.2009.09.012.

[4] Centi G, Perathoner S. Opportunities and prospects in the chemical recycling of carbon dioxide to fuels. Catalysis Today 2009;148:191–205. https://doi.org/10.1016/J.CATTOD.2009.07.075.

[5] Andreas Borgschulte, Noris Gallandat, Benjamin Probst, Riccardo Suter, Elsa Callini, Davide Ferri, et al. Sorption enhanced CO 2 methanation. Physical

Chemistry Chemical Physics 2013;15:9620–5.
https://doi.org/10.1039/C3CP51408K.

[6] Darensbourg DJ, Bauch CG, Ovalles C. Mechanistic aspects of catalytic carbon dioxide methanation. Reviews in Inorganic Chemistry 1985;7:315–40. https://doi.org/10.1515/REVIC.1985.7.4.315.

[7] van Herwijnen T, van Doesburg H, de Jong WA. Kinetics of the methanation of CO and CO2 on a nickel catalyst. Journal of Catalysis 1973;28:391–402. https://doi.org/10.1016/0021-9517(73)90132-2.

[8] Su X, Xu J, Liang B, Duan H, Hou B, Huang Y. Catalytic carbon dioxide hydrogenation to methane: A review of recent studies. Journal of Energy Chemistry 2016;25:553–65. https://doi.org/10.1016/j.jechem.2016.03.009.

[9] Schaaf T, Grünig J, Schuster MR, Rothenfluh T, Orth A. Methanation of CO2 - storage of renewable energy in a gas distribution system. Energy, Sustainability and Society 2014;4. https://doi.org/10.1186/s13705-014-0029-1.

[10] Weatherbee GD, Bartholomew CH. Hydrogenation of CO, on Group VIII Metals I. Specific Activity of Ni/SiO. vol. 68. 1981.

[11] Fujita S-I, Nakamura M, Doi T, Takezawa N. Mechanisms of methanation of carbon dioxide and carbon monoxide over nickel/alumina catalysts. 1993.

[12] Erhan Aksoylu A, İlsenÖnsan Z. Hydrogenation of carbon oxides using coprecipitated and impregnated Ni/Al2O3 catalysts. Applied Catalysis A: General 1997;164. https://doi.org/10.1016/S0926-860X(97)00151-8.

[13] Ocampo F, Louis B, Roger AC. Methanation of carbon dioxide over nickel-based Ce0.72Zr0.28O2 mixed oxide catalysts prepared by sol-gel method. Applied Catalysis A: General 2009;369:90–6. https://doi.org/10.1016/j.apcata.2009.09.005.

[14] Tada S, Shimizu T, Kameyama H, Haneda T, Kikuchi R. Ni/CeO2 catalysts with high CO2 methanation activity and high CH4 selectivity at low temperatures. International Journal of Hydrogen Energy 2012;37:5527–31. https://doi.org/10.1016/j.ijhydene.2011.12.122.

[15] Liu J, Yu J, Su F, Xu G. Intercorrelation of structure and performance of Ni–Mg/Al $_2$ O $_3$ catalysts prepared with different methods for syngas methanation. Catal Sci Technol 2014;4. https://doi.org/10.1039/C3CY00601H.

[16] Muroyama H, Tsuda Y, Asakoshi T, Masitah H, Okanishi T, Matsui T, et al. Carbon dioxide methanation over Ni catalysts supported on various metal oxides. Journal of Catalysis 2016;343:178–84. https://doi.org/10.1016/j.jcat.2016.07.018.

[17] Zhou G, Liu H, Cui K, Xie H, Jiao Z, Zhang G, et al. Methanation of carbon dioxide over Ni/CeO2 catalysts: Effects of support CeO2 structure. International Journal of Hydrogen Energy 2017;42:16108–17. https://doi.org/10.1016/j.ijhydene.2017.05.154.

[18] Atzori L, Cutrufello MG, Meloni D, Cannas C, Gazzoli D, Monaci R, et al. Highly active NiO-CeO2 catalysts for synthetic natural gas production by CO2 methanation. Catalysis Today 2018;299:183–92. https://doi.org/10.1016/j.cattod.2017.05.065.

[19] Mihet M, Lazar MD. Methanation of CO2 on Ni/ γ -Al2O3: Influence of Pt, Pd or Rh promotion. Catalysis Today 2018;306:294–9. https://doi.org/10.1016/j.cattod.2016.12.001.

[20] Riani P, Valsamakis I, Cavattoni T, Sanchez Escribano V, Busca G, Garbarino G. Ni/SiO2-Al2O3 catalysts for CO2 methanation: Effect of La2O3 addition.

Applied Catalysis B: Environmental 2021;284.
https://doi.org/10.1016/j.apcatb.2020.119697.

[21] Garbarino G, Riani P, Magistri L, Busca G. A study of the methanation of carbon dioxide on Ni/Al2O 3 catalysts at atmospheric pressure. International Journal of Hydrogen Energy 2014;39:11557–65.
https://doi.org/10.1016/j.ijhydene.2014.05.111.

[22] Garbarino G, Bellotti D, Riani P, Magistri L, Busca G. Methanation of carbon dioxide on Ru/Al2O3 and Ni/Al2O3 catalysts at atmospheric pressure: Catalysts activation, behaviour and stability. International Journal of Hydrogen Energy 2015;40:9171–82. https://doi.org/10.1016/j.ijhydene.2015.05.059.

[23] Lin J, Ma C, Wang Q, Xu Y, Ma G, Wang J, et al. Enhanced low-temperature performance of CO2 methanation over mesoporous Ni/Al2O3-ZrO2 catalysts. Applied Catalysis B: Environmental 2019;243:262–72.
https://doi.org/10.1016/J.APCATB.2018.10.059.

[24] Guilera J, del Valle J, Alarcón A, Díaz JA, Andreu T. Metal-oxide promoted Ni/Al2O3 as CO2 methanation micro-size catalysts. Journal of CO2 Utilization 2019;30:11–7. https://doi.org/10.1016/J.JCOU.2019.01.003.

[25] Tada S, Ikeda S, Shimoda N, Honma T, Takahashi M, Nariyuki A, et al. Sponge Ni catalyst with high activity in CO2 methanation. International Journal of Hydrogen Energy 2017;42:30126–34. https://doi.org/10.1016/j.ijhydene.2017.10.138.

[26] Huang YH, Wang JJ, Liu ZM, Lin GD, Zhang H bin. Highly efficient Ni-ZrO2 catalyst doped with Yb2O3 for co-methanation of CO and CO2. Applied Catalysis A: General 2013;466:300–6. https://doi.org/10.1016/J.APCATA.2013.06.021.

[27] Yamasaki M, Habazaki H, Yoshida T, Akiyama E, Kawashima A, Asami K, et al. Compositional dependence of the CO2 methanation activity of Ni/ZrO2 catalysts prepared from amorphous NiZr alloy precursors. Applied Catalysis A: General 1997;163:187–97. https://doi.org/10.1016/S0926-860X(97)00142-7.

[28] da Silva DCD, Letichevsky S, Borges LEP, Appel LG. The Ni/ZrO 2 catalyst and the methanation of CO and CO 2. International Journal of Hydrogen Energy 2012;37:8923–8. https://doi.org/10.1016/j.ijhydene.2012.03.020.

[29] Oshima K, Honma Y, Kinoshita K, Gao Z, Honma T, Tada S, et al. Mechanochemical Effect in Mixing Sponge Copper with Amorphous ZrO2

Creates Effective Active Sites for Methanol Synthesis by CO2 Hydrogenation. Journal of Physical Chemistry C 2021;125:8155–62. https://doi.org/10.1021/acs.jpcc.0c10917.

[30] Jia X, Zhang X, Rui N, Hu X, Liu C jun. Structural effect of Ni/ZrO2 catalyst on CO2 methanation with enhanced activity. Applied Catalysis B: Environmental 2019;244:159–69. https://doi.org/10.1016/j.apcatb.2018.11.024.

[31] Cai M, Wen J, Chu W, Cheng X, Li Z. Methanation of carbon dioxide on Ni/ZrO2-Al2O 3 catalysts: Effects of ZrO2 promoter and preparation method of novel ZrO2-Al2O3 carrier. Journal of Natural Gas Chemistry 2011;20:318–24. https://doi.org/10.1016/S1003-9953(10)60187-9.

[32] Ando H, Fujiwara M, Matsumura Y, Tanaka M, Souma Y. Catalytic hydrogenation of carbon dioxide over LaNi 5 activated during the reaction. Journal of Molecular Catalysis A: Chemical 1999;144:117–22.

[33] Rivero-Mendoza DE, Stanley JNG, Scott J, Aguey-Zinsou KF. An alumina-supported ni-la-based catalyst for producing synthetic natural gas. Catalysts 2016;6. https://doi.org/10.3390/catal6110170.

[34] Hirata N, Watanabe R, Fukuhara C. Performance characteristics of auto-methanation using Ru/CeO2 catalyst, autonomously proceeding at room temperature. Fuel 2020;282. https://doi.org/10.1016/j.fuel.2020.118619.

[35] Fukuhara C, Kamiyama A, Itoh M, Hirata N, Ratchahat S, Sudoh M, et al. Auto-methanation for transition-metal catalysts loaded on various oxide supports: A novel route for CO2 transformation at room-temperature and atmospheric pressure. Chemical Engineering Science 2020;219. https://doi.org/10.1016/j.ces.2020.115589.

[36] Mori S, Xu WC, Ishidzuki T, Ogasawara N, Imai J, Kobayashi K. Mechanochemical activation of catalysts for CO2 methanation. Applied Catalysis A: General 1996;137:255–68. https://doi.org/10.1016/0926-860X(95)00319-3.

[37] Yatagai K, Shishido Y, Gemma R, Boll T, Uchida HH, Oguri K. Mechanochemical CO2 methanation over LaNi-based alloys. International Journal of Hydrogen Energy 2020;45:5264–75. https://doi.org/10.1016/j.ijhydene.2019.07.055.

[38] Sawahara K, Gemma R. In-situ monitoring of CO2 methanation: pressure change upon ball-milling of LaNi5 under CO2 and H2. Journal of Advanced Science 2021;33:33107 (in Japanese).

[39] Yatagai K, Gemma R, Uchida H-H, Oguri K. Methanation of CO2 by using LaNi5 alloy with ball-milling method. Journal of Advanced Science 2019;31:31101 (in Japanese).

[40] Soga K, Ikeda S, Imamura H. Hydrogenation of Ethylene over LaNI5 Alloy. n.d.

[41] Tsukuda R, Kojima T, Okuyama D, Kameoka S, Nishimura C, Tsai AP. Hydrogenation of acetylene and propyne over hydrogen storage ErNi5-xAlx alloys and the role of absorbed hydrogen. International Journal of Hydrogen Energy 2020;45:19226–36. https://doi.org/10.1016/j.ijhydene.2020.05.062.

[42] Kato S, Matam SK, Kerger P, Bernard L, Battaglia C, Vogel D, et al. The Origin of the Catalytic Activity of a Metal Hydride in CO2 Reduction. Angewandte Chemie - International Edition 2016;55:6028–32. https://doi.org/10.1002/anie.201601402.

[43] Sawama Y, Niikawa M, Yabe Y, Goto R, Kawajiri T, Marumoto T, et al. Stainless-steel-mediated quantitative hydrogen generation from water under ball milling conditions. ACS Sustainable Chemistry and Engineering 2015;3:683–9. https://doi.org/10.1021/sc5008434.

[44] Hirosaki N, Ogata S, Kocer C. A b initio calculation of the crystal structure of the lanthanide Ln O 2 3 sesquioxides. vol. 351. 2003.

[45] Shi S, Li C, Tang W. Crystallographic and electrochemical performances of La-Mg-Ni-Al-Mo-based alloys as anode materials for nickel-metal hydride batteries. Journal of Alloys and Compounds 2009;476:874–7. https://doi.org/10.1016/j.jallcom.2008.09.152.

[46] Tang C, Du Y, Zhou H. The phase equilibria of the Al-Ce-Ni system at 500 ° C. Journal of Alloys and Compounds 2009;470:222–7. https://doi.org/10.1016/j.jallcom.2008.03.034.

[47] Haglund J, Fernandez Guillermet A, Grimvall G, Korling M. Theory of bonding in transition-metal carbides and nitrides. vol. 48. n.d.

[48] Djerdj I, Garnweitner G, Sheng Su D, Niederberger M. Morphology-controlled nonaqueous synthesis of anisotropic lanthanum hydroxide nanoparticles. Journal of Solid State Chemistry 2007;180:2154–65. https://doi.org/10.1016/j.jssc.2007.05.019.

[49] Attfield JP, Férey G. Structure determinations of La2O2CO3-II and the unusual disordered phase La2O2.52(CO3)0.74Li0.52 using powder diffraction. Journal of Solid State Chemistry 1989;82. https://doi.org/10.1016/0022-4596(89)90232-6.

[50] Huot J, Ravnsbæk DB, Zhang J, Cuevas F, Latroche M, Jensen TR. Mechanochemical synthesis of hydrogen storage materials. Progress in Materials Science 2013;58:30–75. https://doi.org/10.1016/j.pmatsci.2012.07.001.

[51] Honjo T, Nobuki T, Kuji T. Magnetic Properties of Carbon Composite Material Prepared by Ball-Milling. Journal of Japan Society Powder Metallurgy 2009;57:3–9.

[52] Siegmann HC, Schlapbach L, Brundle CR. Self-Restoring of the Active Surface in the Hydrogen Sponge LaNi5. Phicical Review Letters 1978;40:972–5.

[53] Li JPH, Zhou X, Pang Y, Zhu L, Vovk EI, Cong L, et al. Understanding of binding energy calibration in XPS of lanthanum oxide by: In situ treatment. Physical Chemistry Chemical Physics 2019;21:22351–8. https://doi.org/10.1039/c9cp04187g.

[54] Fleming P, Farrell RA, Holmes JD, Morris MA. The rapid formation of La(OH)3 from La2O3 powders on exposureto water vapor. Journal of the American Ceramic Society 2010;93:1187–94. https://doi.org/10.1111/j.1551-2916.2009.03564.x.

[55] Jiang T, Song J, Huo M, Yang NT, Liu J, Zhang J, et al. La2O3 catalysts with diverse spatial dimensionality for oxidative coupling of methane to produce ethylene and ethane. RSC Advances 2016;6:34872–6. https://doi.org/10.1039/c6ra01805j.

[56] Sunding MF, Hadidi K, Diplas S, Løvvik OM, Norby TE, Gunnæs AE. XPS characterisation of in situ treated lanthanum oxide and hydroxide using tailored charge referencing and peak fitting procedures. Journal of Electron Spectroscopy and Related Phenomena 2011;184:399–409. https://doi.org/10.1016/J.ELSPEC.2011.04.002.

[57] Kang JG, Kim Y il, Won Cho D, Sohn Y. Synthesis and physicochemical properties of La(OH)3 and La2O3 nanostructures. Materials Science in Semiconductor Processing 2015;40:737–43. https://doi.org/10.1016/j.mssp.2015.07.050.

[58] Ramana C v., Vemuri RS, Kaichev V v., Kochubey VA, Saraev AA, Atuchin V v. X-ray photoelectron spectroscopy depth profiling of La 2O 3/Si thin films deposited by reactive magnetron sputtering. ACS Applied Materials and Interfaces 2011;3:4370–3. https://doi.org/10.1021/am201021m.

[59] Stoychev D, Valov I, Stefanov P, Atanasova G, Stoycheva M, Marinova T. Electrochemical growth of thin La 2 O 3 films on oxide and metal surfaces. Materials Science and Engineering C 2003;23:123–8.

[60] Boukha Z, Fitian L, López-Haro M, Mora M, Ruiz JR, Jiménez-Sanchidrián C, et al. Influence of the calcination temperature on the nano-structural properties, surface basicity, and catalytic behavior of alumina-supported lanthana samples. Journal of Catalysis 2010;272:121–30. https://doi.org/10.1016/j.jcat.2010.03.005.

[61] Uwamino Y, Ishizuka T, Yamatera H. X-ray photoelectron spectroscopy of rare-earth compounds. Journal of Electron Spectroscopy and Related Phenomena 1984;34. https://doi.org/10.1016/0368-2048(84)80060-2.

[62] Shelef M, Haack LP, Soltis RE, Devries JE, Logothetis EM. An XPS Study of Interactions in Thin Films Containing a Noble Metal with Valence-lnvariant and Reducible Oxides. vol. 137. 1992.

[63] Phillips SL, Hale F v, Silvester LF, Siegel MD. Thermodynamic Tables for Nuclear Waste Isolation. Vol 1. Aqueous Solutions Database. 1988.

[64] Neumann A, Walter D. The thermal transformation from lanthanum hydroxide to lanthanum hydroxide oxide. Thermochimica Acta 2006;445:200–4. https://doi.org/10.1016/j.tca.2005.06.013.

[65] TOKUMITSU K. Reduction of metal oxides by mechanical alloying method. Solid State Ionics 1997;101–103:25–31. https://doi.org/10.1016/S0167-2738(97)84004-0.

[66] Suzuki K, Ishikawa K, Aoki K. Degradation of LaNi5 and LaNi4.7Al0.3 hydrogen-absorbing alloys by cycling. Materials Transactions, JIM 2000;41:581–4. https://doi.org/10.2320/matertrans1989.41.581.